THE ANATOMICAL RECORD 302:1696–1708 (2019)

Anatomy and Ontogeny of the Mandibular Symphysis in *Alligator mississippiensis*

EMILY J. LESSNER [1]*, CORTAIGA A. GANT,[1] TOBIN L. HIERONYMUS,[2] MATTHEW K. VICKARYOUS,[3] AND CASEY M. HOLLIDAY [1]

[1]Program in Integrative Anatomy, Department of Pathology and Anatomical Sciences, University of Missouri Medical School, Columbia, Missouri

[2]Department of Anatomy and Neurobiology, Northeast Ohio Medical University, Rootstown, Ohio

[3]Department of Biomedical Sciences, University of Guelph, Guelpgh, Ontario, Canada

ABSTRACT

Crocodylians evolved some of the most characteristic skulls of the animal kingdom with specializations for semiaquatic and ambush lifestyles, resulting in a feeding apparatus capable of tolerating high biomechanical loads and bite forces and a head with a derived sense of trigeminal-nerve-mediated touch. The mandibular symphysis accommodates these specializations being both at the end of a biomechanical lever and an antenna for sensation. Little is known about the anatomy of the crocodylian mandibular symphysis, hampering our understanding of form, function, and evolution of the joint in extant and extinct lineages. We explore mandibular symphysis anatomy of an ontogenetic series of *Alligator mississippiensis* using imaging, histology, and whole mount methods. Complex sutural ligaments emanating about a midline-fused Meckel's cartilage bridge the symphysis. These tissues organize during days 37–42 of *in ovo* development. However, interdigitations do not manifest until after hatching. These soft tissues leave a hub and spoke-like bony morphology of the symphyseal plate, which never fuses. Interdigitation morphology varies within the symphysis suggesting differential loading about the joint. Neurovascular canals extend throughout the mandibles to alveoli, integument, and bone adjacent to the symphysis. These features suggest the *Alligator* mandibular symphysis offers compliance in an otherwise rigid skull. We hypothesize a fused Meckel's cartilage offers stiffness in hatchling mandibles prior to the development of organized sutural ligaments and mineralized bone while offering a scaffold for somatic growth. The porosity of the dentaries due to neurovascular tissues likely allows transmission of sensory and proprioceptive information from the surroundings and the loaded symphysis. Anat Rec, 302:1696–1708, 2019. © 2019 American Association for Anatomy

Key words: Meckel's cartilage; sutural ligament; feeding apparatus; trigeminal

Grant sponsor: National Science Foundation Division of Earth Sciences; Grant number: NSF EAR 1631684; Grant sponsor: Missouri Research Board, University of Missouri Life Sciences Fellowship Program (to EJL), IMSD-Express Fellowship (to CAG), Department of Pathology and Anatomical Sciences, University of Missouri School of Medicine.

*Correspondence to: Emily J. Lessner, Program in Integrative Anatomy, Department of Pathology and Anatomical Sciences, University of Missouri Medical School, Columbia, MO, 65212. E-mail: ejlessner@mail.missouri.edu

Received 26 September 2018; Revised 14 November 2018; Accepted 10 December 2018.

DOI: 10.1002/ar.24116

Published online 18 March 2019 in Wiley Online Library (wileyonlinelibrary.com).

The mandibular symphysis is the characteristic linkage between the mandibles of gnathostome vertebrates. The symphysis takes a variety of forms among tetrapods, spanning a spectrum of morphologies ranging from the coossified beaks and mandibles of turtles, birds, and primates, to variably sutured symphyses in artiodactyl and carnivoran mammals and the relatively open joints in lepidosaurs and amphibians (Scapino, 1981; Hogg, 1983; Hogue and Ravosa, 2001; Svensson and Haas, 2005; Herring et al., 2008; Williams et al., 2008; Holliday et al., 2010; Holliday and Nesbitt, 2013). The symphysis is composed of a diversity of skeletal tissues that reflect the biomechanical environment of the joint as well as a diversity of neurovascular structures that supply and innervate the integument capping the dentaries (Bellairs, 1984; Kley, 2006; Holliday et al., 2010). Here, we describe these tissues in the mandibular symphysis of *Alligator mississippiensis* during various stages of development.

Alligators and other crocodylians possess numerous adaptations for predatory behavior including flat, torsion-resistant skulls (Busbey, 1995), large jaw muscles (Busbey, 1989), enlarged pterygoid flanges that stabilize the lower jaws (Porro et al., 2011), and highly resistant polyphydont teeth (Erickson et al., 2012). Linking these features together are the craniomandibular joints, whose structural and physiological significance remains to be thoroughly understood. Although Bailleul and Holliday (2017) documented histological features of the otic and jaw joints, little remains understood about how other cranial joints are built, in particular the mandibular symphysis, a biomechanically and physiologically important articulation. Insight into the anatomical organization of this joint in *A. mississippiensis* leads to a broadened understanding of the biomechanical environment of the entire skull.

Alligator ontogeny is highlighted by a progressive suite of musculoskeletal changes that enable them to generate the highest bite forces known and feed on large prey items (Erickson et al., 2003; Sellers et al., 2017). A detailed understanding of cranial joint structure is therefore critical to understanding how they achieve this feat. Alligator mandibular symphyses experience significant torsion and dorsoventral shear due to the long axis rotation and medial flexion of the mandibles—thus the jaws, along with their inclusive joints, are under selective pressures for optimized performance (Porro et al., 2011). Additionally, during ontogeny, the alligator snout elongates and tooth shape changes in parallel to shifts in ecological niche and feeding ecology (Erickson et al., 2003; Walmsley et al., 2013; Sellers et al., 2017). How the symphyseal joint and Meckel's cartilage withstand and react to the complex forces related to these shifts in feeding remains to be investigated. Our description lends an anatomical basis on which to found hypotheses of feeding ecology.

Crocodylians possess characteristically interdigitating bony mandibular symphyses that never coossify and fuse (Holliday and Nesbitt, 2013). This pattern holds for brevisymphyseal caimans as well as longisymphyseal gharials and crocodiles. Each crocodylian symphyseal plate possesses numerous ossified sutural fins that radiate from a mid-ventrally-situated fossa excavated by Meckel's cartilage (Holliday and Nesbitt, 2013). Although this spoke and hub morphology is consistent among crocodylians, its exact morphology varies depending on the shape and length of the mandibular symphysis (Jacoby et al., 2015). To date, little is known about the sutural ligaments, cartilages, and other connective tissues that span this joint.

These biomechanical modifications evolved with an equally highly derived somatosensory system requiring rather porous bone to accommodate the dendritic assemblage of alveolar neurovascular bundles (Leitch and Catania, 2012; Di-Poï and Milinkovitch, 2013). These branches of the mandibular division of the trigeminal nerve conduct sensory impulses from the heavily innervated skin and are accompanied by branches from the mandibular and oromandibular arteries and veins (Leitch and Catania, 2012; George and Holliday, 2013; Porter et al., 2016). These neurovascular bundles perforate the bony mandible and emerge on the external surface through many small foramina that characterize the crocodylian rostrum (Soares, 2002; Leitch and Catania, 2012). Despite these gross understandings, the internal anatomy of the mandibles, including the courses, density, and targets of neurovasculature remain undocumented in alligator symphysis as well as other reptilian taxa.

Better understanding of the structure and function of the alligator mandibular symphysis is necessary to understand function and evolution of the crocodyliform skull. The rich paleodiversity of crocodyliforms, and suchians in general, reflects the importance of biomechanical and sensory adaptations of the rostrum as the clade experienced radiations of astounding morphological diversity during the Mesozoic era, filling numerous trophic niches (Clark et al., 2004; Stubbs et al., 2013). Crocodyliforms evolved an incredible diversity of cranial shapes, including species arguably capable of derived chewing behaviors quite different from those of the modern clade of extant crocodylians (Nobre et al., 2008; Ősi and Weishampel, 2009; O'Connor et al., 2010). Much of the cranial variability of this group is present in the rostrum rather than the neurocranial region (Brochu, 2001). Thus, following our initial description of the symphyseal morphology of *Alligator*, we expect these findings will shed light on the biology and evolution of *Alligator* as well as other crocodyliforms and reptiles.

MATERIALS AND METHODS

Specimens

Fresh-frozen cadaverous hatchling and adult specimens of *A. mississippiensis* Daudin 1802 were obtained from Rockefeller State Refuge, (Grand Chenier, Louisiana) (Table 1). In addition, eggs, embryos, and hatchlings from Rockefeller State Refuge were incubated and collected at University of Missouri as per University of Missouri Animal Care and Use Committee protocol (ACUC 7477). Embryos were staged as per Ferguson (1985), euthanized, and collected from days 37 to 50, and immediately following hatching. Specimens were either immediately fixed in 10% neutral buffered formalin (NBF) and stored in 70% ethanol or frozen for later use.

Computed Tomography Scanning

One specimen, accessioned into the University of Missouri Vertebrate Collections as MUVC AL31 and featured in Holliday and Nesbitt (2013) and George and Holliday (2013), was immersed in 10% iodine potassium iodide (I_2KI) for 5 weeks. The specimen was scanned at the University of Missouri Biomolecular Imaging Center on a Siemens Inveon MicroCT scanner using 80 kV, 500 mA, and

TABLE 1. Specimen numbers and ages of specimens figured

Taxa	Specimen number	Age	Ferguson stage
Alligator mississippiensis	MUVC AL1	3 years	–
Alligator mississippiensis	MUVC AL008	Unknown	–
Alligator mississippiensis	MUVC AL809	10 months	–
Alligator mississippiensis	MUVC AL31	3 months	–
Alligator mississippiensis	MUVC AL32	3 months	–
Alligator mississippiensis	MUVC AL106	Unknown	–
Alligator mississippiensis	MUVC AL114	50-day embryo	24
Alligator mississippiensis	MUVC AL133	39-day embryo	22
Alligator mississippiensis	MUVC AL134	38-day embryo	22
Alligator mississippiensis	MUVC AL135	37-day embryo	22
Alligator mississippiensis	MUVC AL136	38-day embryo	22
Alligator mississippiensis	MUVC AL137	45-day embryo	23
Crocodylus niloticus madagascariensis	Handschuh et al., 2010	50-day embryo	22–25
Crocodylus moreletii	TMM M-4980	Unknown	–
Crocodylus johnstoni	TMM M-6807	Unknown	–

slice thickness of 83 μm. The same specimen was later reimmersed in I_2KI and rescanned on a Zeiss Xradia Versa 510 using 120 kV, 0.083 mA, and slice thickness of 39.42 μm for higher resolution images of soft tissues (e.g., bone, teeth, sutural ligament, Meckel's cartilage, and trigeminal nerve) (Gignac et al., 2016). An additional specimen, MUVC AL008, was scanned at the University of Missouri School of Medicine Department of Radiology on a Siemens Somatom Definition Scanner. Scan data were imported as DICOM files into Avizo v. 9.5 for segmentation. Anatomical structures were segmented manually using both magic wand and paintbrush tools. Screen captures of specific slices and .surf files were taken from Avizo. Segmented structures were saved as .obj files, imported into Autodesk Maya, and exported and uploaded into Sketchfab as a 3D interactive model (https://sketchfab.com/3d-models/be5ad1702745465ab24ea5e7aee66bc3). MUVC scan data (MUVC AL 008, MUVC AL 031) are available from Open Science Framework (https://osf.io/jmpck/). *Crocodylus johnstoni* (TMM M-6807) and *Crocodylus moreletii* (TMM M-4980) computed tomography scans were obtained from DigiMorph.org.

Histology

For histology, mandibular symphysis specimens were harvested using a rotary Dremel tool. The largest specimen (AL1) was processed for thick-section plastic sectioning as described in Holliday et al. (2010) and Payne et al. (2011). Briefly, the specimen was infiltrated with methyl methacrylate (MMA) and dibutyl phthalate (DBP) followed by embedding in fresh MMA, DBP, and Perkadox-16 and allowed to polymerize for 2 weeks. Once set, thick 100 μm slides were cut using an EXAKT Cutting and Grinding System (EXAKT Technologies, Oklahoma City, OK) and then polished to a final thickness of 25–35 μm. These slides were then stained using Sanderson's Rapid Bone Stain and Van Giesons's Picrofuchsin.

Smaller specimens of an ontogenetic series of *Alligator* (MUVC: AL32, AL106, AL114, AL133, AL134) were processed for standard paraffin histology. Prior to processing, tissues were decalcified for 30 min in Cal-Ex® (Fisher Scientific, Hampton, NH), then dehydrated in 100% isopropanol, cleared in xylene and infiltrated with paraffin wax using an automated processor (Fisher Scientific). Embedded tissues were then sectioned at 5 μm using a rotary microtome at the University of Missouri Veterinary Medicine Diagnostic Laboratory (Leica RM255 microtome, Wetzlar, Germany) or at the University of Guelph Department of Biomedical Sciences (HM 355S Automatic Microtome, Thermo Fisher Scientific), and the sections were mounted on charged slides (Surgipath X-tra; Leica Microsystems) and baked at 60 °C overnight.

To differentiate fibrous connective tissue and skeletal muscle, representative slide-mounted sections were stained with a modified Masson's trichrome (Witten and Hall, 2003; see also McLean and Vickaryous, 2011). Briefly, sections were brought to water using three rinses in xylene (2 min each), three rinses in absolute (100%) isopropanol (2 min each), one rinse of 70% isopropanol (2 min), and then rinsed in deionized water (1 min). Sections were then stained with Mayer's hematoxylin (10 min), blued in ammonia water (~15 sec), and rinsed with deionized water. Sections were then stained in 0.5% ponceau xylidine/0.5% acid fuschin in 1% acetic acid solution (2 min), rinsed in deionized water, stained in 1% phosphomolybdic acid (10 min), rinsed in deionized water, stained in 2% light green (90 sec), and rinsed in deionized water. Slides were then rinsed in 95% isopropanol (2 min) followed by three rinses in absolute isopropanol (2 min each), and cleared with three rinses in xylene (2 min each). Slides were coverslipped using Cytoseal (Fisher Scientific).

To stain for glycosaminoglycans (characteristic of cartilage), we used safranin O counterstained with fast green. Sections were brought to water (as above), and stained with Weigert's hematoxylin (8–10 min), followed by rinsing with gentle running tap water (5 min). Sections were then stained with 0.05% fast green (60 sec), rinsed in 1% acetic acid (1 min), and stained with 0.1% safranin O (10 min), after which sections were dehydrated and coverslipped (as above).

To stain for collagen, we used picrosirius red (PSR) (Junqueira et al., 1979). Sections were brought to water (as above), and stained with Weigert's hematoxylin (8 min), followed by rinsing with gentle running tap water (10 min). Sections were then stained with picrosirius red solution (1 hr), and rinsed in 0.5% acetic acid (1 min), after which sections were dehydrated and coverslipped (as above).

Unstained specimens and those stained with PSR were studied using polarized light on Olympus CX31 and

Nikon Eclipse 50i compound microscopes. Other slides were viewed using an Aperio Slide Scanner, a Nikon SMZ dissection scope, or an Olympus CX31 microscope with Pixelink camera.

Whole-Mount Staining

For bone and cartilage staining, an ontogenetic series of *Alligator* (MUVC: AL135, AL136, AL137) were skinned, eviscerated, and fixed in 10% NBF. Specimens were dehydrated in ethanol (15%, 40%, 70%, 95%) for 2–4 hr per concentration then transferred to acetone with light agitation. For cartilage staining, specimens were placed in a solution of Alcian blue (11 mg alcian blue, 77.5 mL 95% ethanol, and 22.5 mL acetic acid) for up to 48 hr then dehydrated in multiple solutions of 95% ethanol for up to 48 hr. For clearing, specimens were rehydrated (95%, 70%, 40%, 15% ethanol) and then placed in water for 2–4 hr per concentration before incubating in an enzymatic solution (30 mL saturated aqueous sodium tetraborate, 70 mL distilled water, 1 g 4 × pancreatin) in a 37 °C water bath until the skeleton became visible (solution changes every 4–5 days). For bone staining, specimens were placed in a solution of Alizarin red (15 drops 0.1% alizarin red S and 100 mL 0.5% KOH) for 1–2 days until bones were stained deep red. Final clearing was by immersion in a 0.5% KOH/glycerol series (3:1, 1:1, 1:3, pure glycerol) for 1–5 days per stage. Specimens were stored in 100% glycerol.

To whole-mount nerves, we used the Sudan Black B protocol of Filipski and Wilson (1986). Alligator specimen MUVC AL809 was fixed in 10% NBF for 4 weeks. Following fixation, the head was removed and immersed in distilled water for 1 week, bleached in 10% hydrogen peroxide for 2 days, and macerated in 30% saturated sodium borate solution with 0.5 g of trypsin for 4 weeks with solution changes every week. After maceration, the specimen was immersed in water for 10 min, followed by 70% ethanol for 15 min, and Sudan Black B stain solution for 25 min. The Sudan Black B stain was prepared by combining 0.5 g Sudan Black B stain with 100 mL of 70% ethanol in a warm water bath for 2 days then filtering. Excess stain was removed by soaking in 5–10 min increments in solutions of 70% ethanol until stained nerve fibers were visible. Final clearing was performed by immersion in distilled water for 1 day, 40% glycerol for 6 hr, and 70% glycerol for 1 day. Specimens were stored in 100% glycerol. Specimens were viewed and photographed using a Nikon SMZ100 microscope, Nikon Digital Sight U2/L2 camera, and NIS-Elements F v 4.30.01 software.

RESULTS

Observations from all specimens were combined in the following description of mandibular symphysis gross morphology. The symphysis of *A. mississippiensis* comprises multiple tissue domains including integument, bone, Meckel's cartilage, sutural ligament, and neurovasculature (Figs. 1 and 2; Table 2). The dentaries meet at the midline at the symphyseal plate, which is oval in shape in the midsagittal plane. In the axial plane, the bony portions of the symphyseal plate are expanded dorsoventrally at the midline (e.g., Figs. 2K,P and 3A) but elsewhere the symphysis maintains a uniform dorsoventral height. The overall osteological features of the mandibular symphysis include the medial surface or symphyseal plate, the dorsal alveolar and gingival region, and the rostral, lateral, and ventromedial integumentary surfaces. Both the rostral and lateral integumentary surfaces are perforated by neurovascular foramina. In contrast, the ventromedial surfaces of the dentaries are smooth and covered by loose connective tissue and gular skin associated with the oral and sublingual cavities, as well as the attachment of the rostral portion of m. intermandibularis just deep to these tissues.

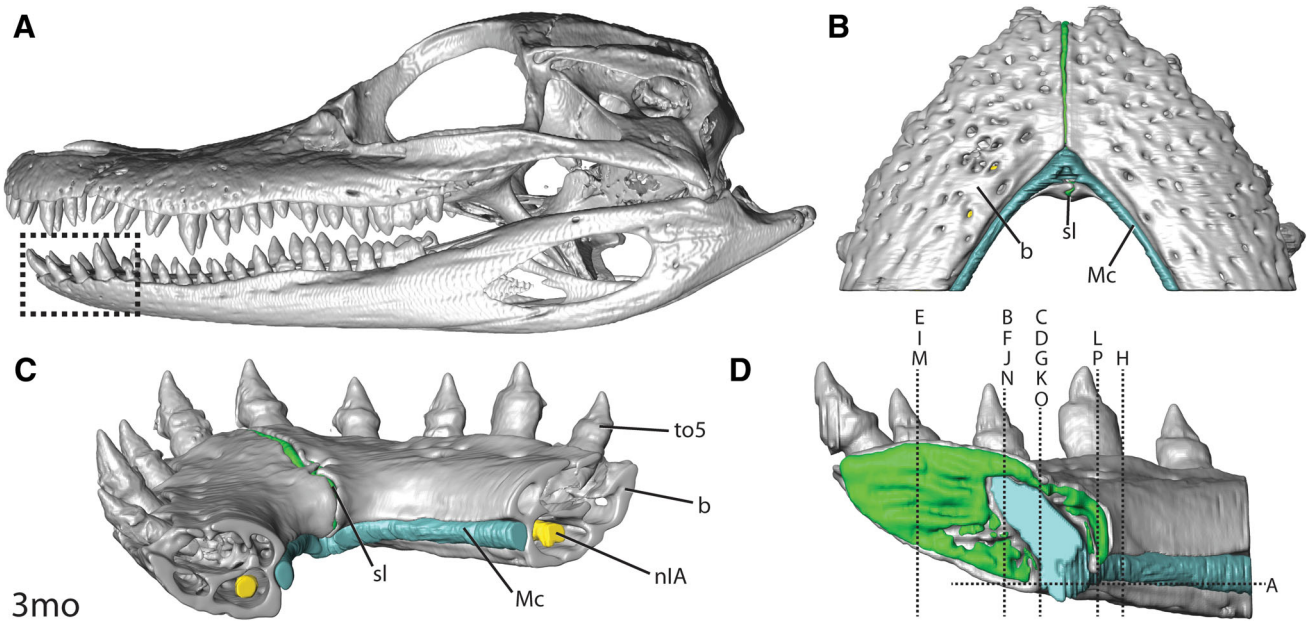

Fig. 1. 3D representation of the skull of 3 month MUVC AL31 in left lateral view **(A)** and close-up views of the symphysis in ventral **(B)**, posterolateral **(C)**, and medial **(D)** views. Location of sections in Figure 2 depicted in (D). Anatomical abbreviations in Table 2.

The caudoventral surface of the bony symphysis possesses a midline bony tubercle associated with the attachment of m. genioglossus. Dorsal to this tubercle is the groove and fossa for Meckel's cartilage (Holliday and Nesbitt, 2013) and the caudal margin of the symphyseal plate. Neurovascular channels perforate the symphyseal plate medially, between the bilateral dentaries. Internally, inferior alveolar neurovascular canals perforate the dentaries, and the dorsal surface of each dentary is further invested with alveoli, periodontal ligaments, and dentition.

Sutural ligament and Meckel's cartilage bridge the contralateral symphyseal plates. Whereas the sutural ligament is present rostrocaudally in the sagittal plane, Meckel's cartilage is most expansive mediolaterally in the axial plane (Figs. 1 and 3A,B). Meckel's cartilage passes continuously from the symphyseal plate along the length of the ventromedial border of each dentary. Each cartilaginous rod is oriented rostrocaudally and is enclosed by the dentary and splenial. Meckel's cartilage continues rostrally, emerging via a foramen at the rostral margin of the splenial, but remains in the Meckelian groove on the ventromedial surface of the dentary just caudal to the symphysis. Right and left Meckelian cartilages fuse in the midline (Figs. 2A,B and 4A–E), eventually forming a dorsoventrally oriented plate-like process within the caudal portion of the symphysis we term the spatulate process. This process has been described as an independent wedge of "basimandibular" cartilage (Parker, 1883) but ontogenetic data presented here suggests that it occurs as a result of fusion of the right and left cartilaginous rods. Development of the spatulate process begins caudally as small dorsolateral extensions of each Meckel's cartilage. Once these cartilages fuse, the now unified spatulate process flattens dorsoventrally and tapers rostrodorsally. This cartilaginous process gradually becomes enclosed within the Meckelian fossa of the dentaries (within the region of the symphyseal plate) and terminates dorsomedial to the roots of the rostral most teeth (Figs. 2A and 3B).

The architecture of the mandibular symphysis develops *in ovo*, primarily during days 37–42 of incubation (Ferguson (1985) Stages 22–23). Meckel's cartilage condenses and elongates rostrally and then medially toward the midline during Stage 22. Simultaneously, the dentaries begin to ossify around the cartilages forming a fossa around the tissues of

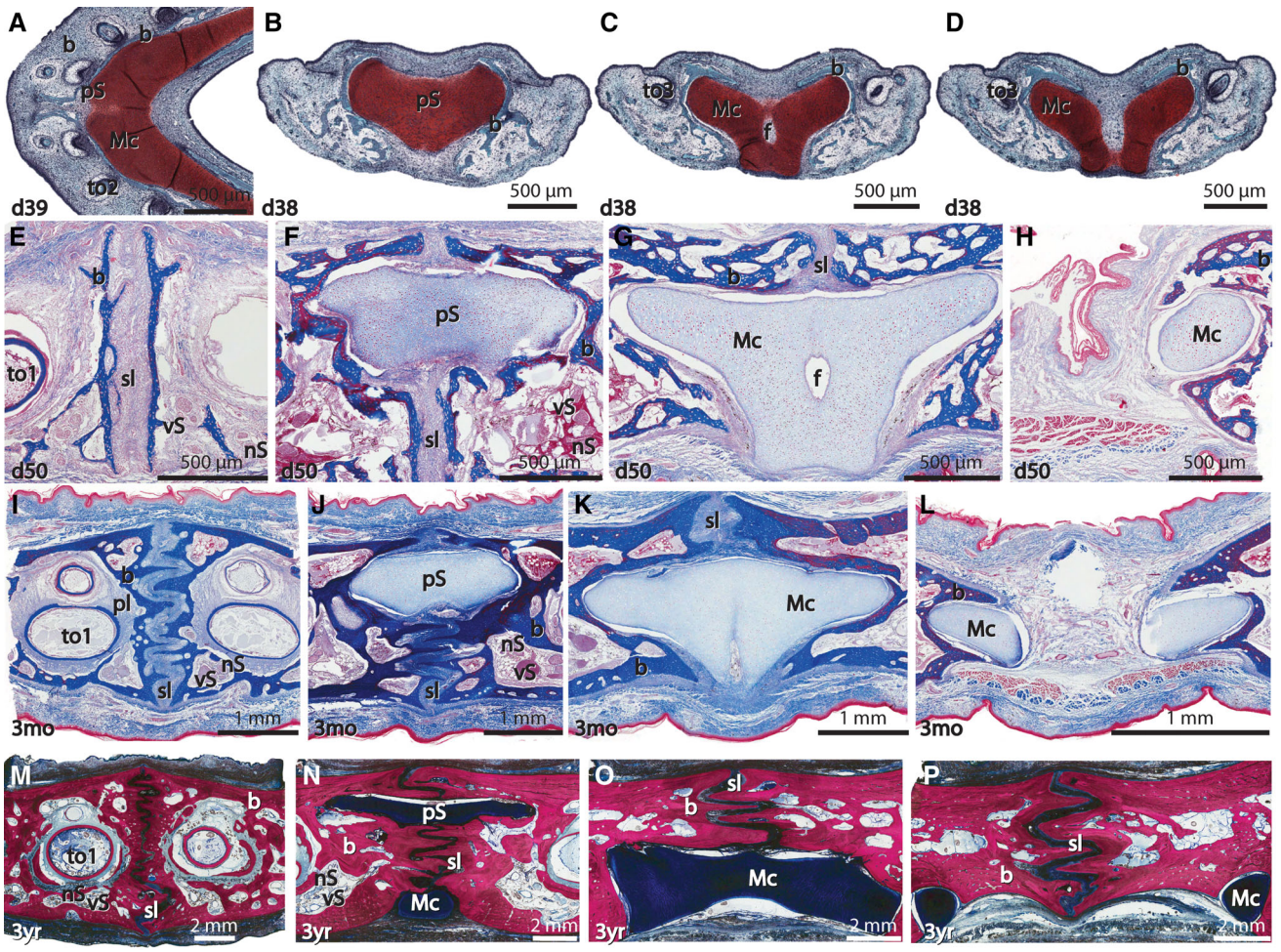

Fig. 2. Serial histological sections from the mandibular symphysis region of *Alligator mississippiensis* in horizontal view of day 39 MUVC AL 133 (**A**; Safranin O-Fast Green), and axial view from rostral (**B**, **E**, **I**, **M**) to caudal (**D**, **H**, **L**, **P**) of day 38 MUVC AL 134 (**B–D**; Safranin O-Fast Green), day 50 MUVC AL114 (**E–H**; Masson's trichrome), 3 month MUVC AL32 (**I–L**; Masson's trichrome), and 3 year MUVC AL1 (**M–P**; alizarin red and toluidine blue). Scale bar = 500 µm A-H; Scale bar = 1 mm I-L; Scale bar = 2 mm M-P. Anatomical abbreviations in Table 2.

the joint. Convergence and fusion of the paired Meckel's cartilages begins at the end of Stage 22 and start of Stage 23 (Fig. 4). Fusion first occurs ventrally between the cartilaginous rods, but fusion in the spatulate process occurs secondarily, sometime after Stage 24. Even in late staged embryos, fusion between the contralateral cartilages is incomplete, leaving a conspicuous fenestra in the midline filled with loose connective tissue (Fig. 2C,G). This fenestra gradually disappears as growth continues posthatching. During Stages 22–24, the spatulate process becomes narrower dorsoventrally and less rounded laterally. As ossification and growth of the dentaries progresses, the spatulate process adopts its final form as a thin sliver of cartilage (Fig. 2N). Compared to hatchlings and adults, there is an increased density of chondrocytes at the edges of Meckel's cartilage in embryos.

TABLE 2. Anatomical abbreviations

Abbreviation	Expansion
b	Bone
f	Fenestra
Mc	Meckel's cartilage
Mf	Meckelian fossa
nIA	Inferior alveolar nerve
nS	Symphyseal nerve
pl	Periodontal ligament
pS	Spatulate process
sl	Sutural ligament
sp	Symphyseal plate
to	Tooth
vS	Symphyseal vasculature

In adult alligators, the surface of the symphyseal plate is marked by a series of bony ridges and grooves radiating from the Meckelian fossa in all directions in the midsagittal plane (Figs. 4F and 6C). Although not quantified, the sutural fins caudal to the Meckelian fossa appear to be shorter, fewer, and invade more deeply into the symphyseal plate than those located rostral to the fossa (Fig. 2). Contact between the dentaries is reinforced by bundles of transversally organized connective tissue fibers, the sutural ligament. Fibers of the sutural ligament are oriented slightly oblique to the axial plane and are subparallel to one another. The collagen fibers of the sutural ligament anchor into the adjacent bone via periosteal Sharpey's fibers (Fig. 5). In addition to the transversely oriented fibers, some fibers also appear to pass into the midsagittal plane of the symphysis, perhaps accommodating the presence of neurovasculature within the sutural ligament. During embryonic development, between Ferguson Stages 22 and 24, (e.g., MUVC: AL133, and AL 114), the bony symphysis begins as a bilateral pair of vertical plates that lack interdigitations and is accompanied by a comparatively disorganized sutural ligament (Fig. 2A,E). Within 3 months of hatching (e.g., MUVC AL31 and AL32), regions of the suture both rostral and caudal to Meckel's cartilage have begun to form bony interdigitations except for the rostralmost and caudalmost extents, respectively (Fig. 2I, J). At 3 years of age (e.g., MUVC AL1), these interdigitations cover the entire symphyseal plate, and collagen fibers of the sutural ligament are densely organized.

Ossification of the symphysis begins around Stage 22 with bone first appearing at the at the rostrolateral edges of Meckel's cartilage and around the alveoli nearest to the spatulate process (Fig. 2A–D). The bone is well ossified by

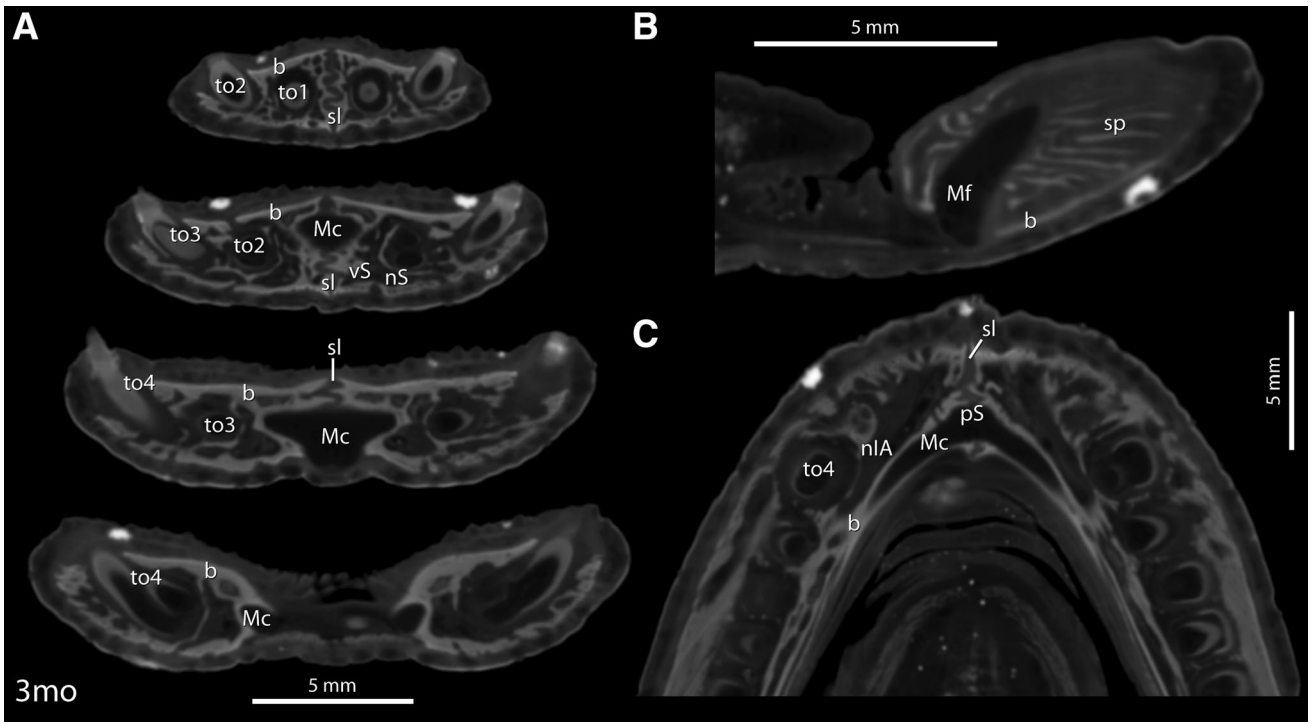

Fig. 3. Serial CT sections of 3 month MUVC AL31 in axial view from rostral (top) to caudal (bottom) **(A)**, in sagittal view at the median of the skull **(B)**, and in horizontal view at the location of fusion of the cartilaginous rods **(C)**. Scale bars = 5 mm. Anatomical abbreviations in Table 2.

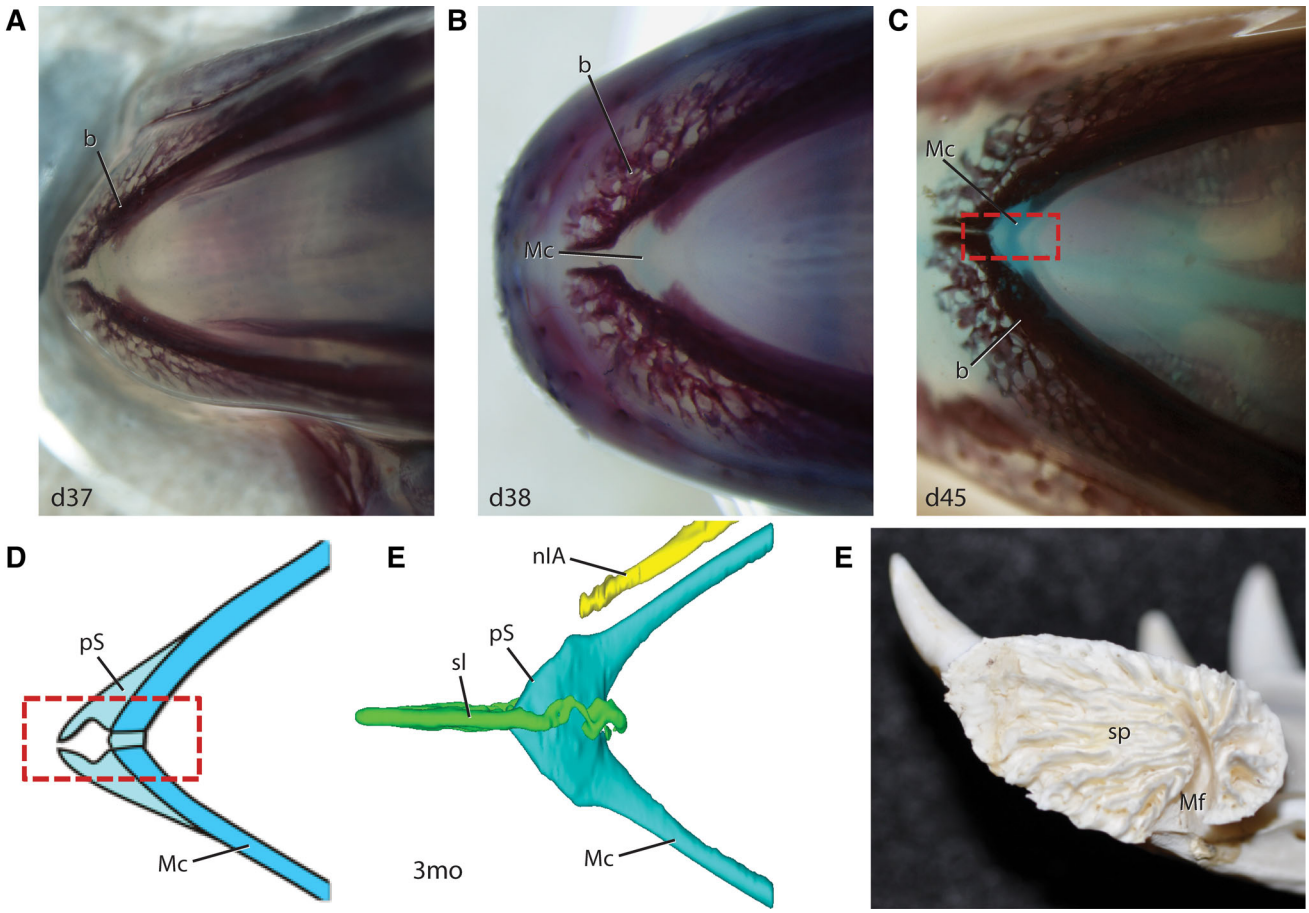

Fig. 4. Progression of fusion of Meckel's cartilage within the mandible of cleared and stained embryonic alligators in ventral view at day 37 (MUVC AL135) **(A)**, at day 38 (MUVC AL136) **(B)**, and day 45 (MUVC AL137) **(C)**, with a 2-D interpretation of the embryonic cartilaginous rods and spatulate process **(D)**, a 3-D representation of the sutural ligament, Meckelian cartilage, and inferior alveolar nerve in dorsal view from CT data of 3 month MUVC AL31 **(E)**, and a medial view of the mandibular symphysis of *Alligator mississippiensis* **(F)**. Anatomical abbreviations in Table 2.

3 months. In the 3-year *A. mississippiensis* (MUVC AL1), osteocytes are in greatest concentrations within the sutural interdigitations (Fig. 2M–P).

Neurovasculature is present in bony canals throughout the rostral portion of the dentaries (Fig. 6). There is evidence of these canals in the Stage 24 *A. mississippiensis* (MUVC AL114), and the minimal bone present in the Stage 22 *A. mississippiensis* (MUVC AL133) wraps around the expected location of the bundles. Beyond Stage 24 (e.g., MUVC AL114, AL31, and AL32), there is a large neurovascular canal present lateral to Meckel's cartilage caudally, the inferior alveolar canal housing the inferior alveolar ramus of the mandibular branch of the trigeminal nerve. This canal subdivides into a larger ventrolateral canal and a smaller dorsolateral canal rostral to the termination of Meckel's cartilage, both extending a number of small symphyseal rami, (Figs. 2 and 7). These canals communicate with the alveoli, innervating mechanoreceptors within the periodontal ligament between the teeth and the bony symphysis (Fig. 7A). These canals also communicate with the sutural ligament, which contains small vessels throughout and potential mechanoreceptors (Fig. 7B–D). The neurovasculature branches out through bony canals to numerous foramina in the dentaries to the integumentary sensory organs evident in the skin covering the dentaries (Fig. 7E,F). Myelinated nerve fibers are visible within the skin crossing the symphysis along the ventral surface of the dentaries (Fig. 6A,B).

DISCUSSION

The mandibular symphysis of *A. mississippiensis* is a morphologically and histologically complex joint, including contributions from a unified Meckel's cartilage, the unfused dentaries, and an elaborate sutural ligament. This arrangement demonstrates an ontogenetic transformation that appears to reflect the influence of mechanical loadings associated with changes in prey-type and feeding behaviors including dorsoventral shearing and transverse twisting and bending ("inverse wishboning" in Porro et al., 2011). Early fusion of Meckel's cartilage may provide structural support while the symphysis develops, allowing the progression in diet from insects and fish, to crustaceans and small vertebrates, to large mammals and turtles (Kellogg, 1929).

The differences in interdigitation of the suture relative to the Meckelian fossa are likely a result of the bending loads experienced during interaction with struggling prey.

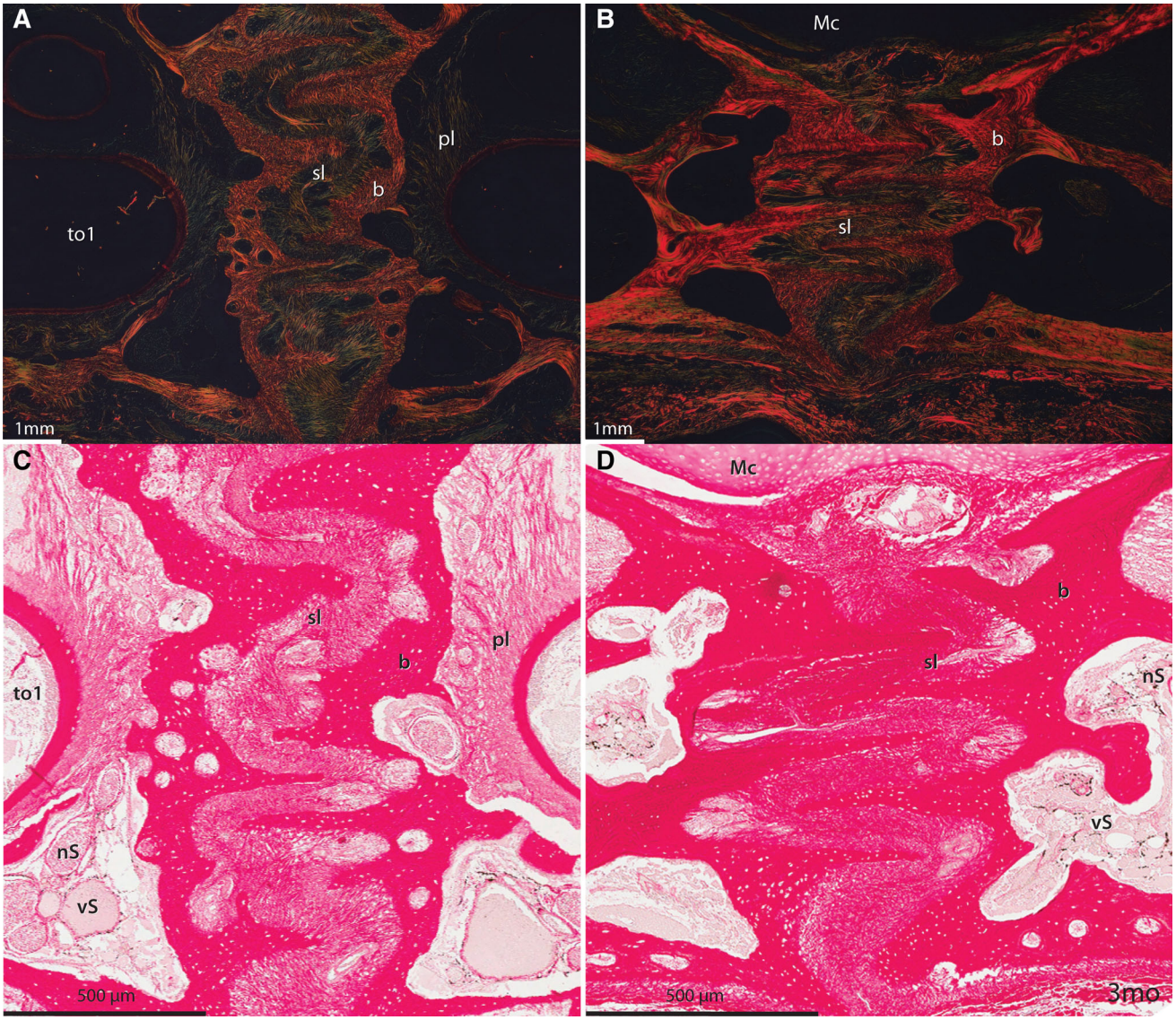

Fig. 5. Polarized light histological sections in axial view of 3 month MUVC AL32 (**A**, **B**) with accompanying picrosirius red sections (**C**, **D**) from the rostral (A, C) and caudal (B, D) portion of the mandibular symphysis of *Alligator mississippiensis*. Scale bar = 1 mm A, B; scale bar = 500 µm C, D. Anatomical abbreviations in Table 2.

As the caudal mandible is pulled medially by jaw muscles, the symphysis experiences compressive forces at the caudal portion of the joint and tension at the rostral portion of the joint (Porro et al., 2011, 2013). Compressive strain has been correlated to the extent of interdigitation (Rafferty and Herring, 1999), and therefore, the deep and shallow interdigitations of the caudal and rostral portions of the suture reflect the compressive and tensile forces, respectively. As bone is stronger in compression than in tension (Currey, 2002), the presence of more surface devoted to bone and collagen at the rostral portion of the joint is likely indicative of the tension experienced there. The collagen fibers within the suture are also oriented to resist these forces. At the tips of the bony interdigitations in the rostral portion of the *Alligator* symphysis, fibers are generally oriented for tension-resistance as hypothesized by Scapino (1981) and Rafferty and Herring (1999) (Figs. 1B and 5). In the caudal portion of the *Alligator* symphysis, the fiber orientations are less organized (Langston, 1973; Busbey, 1989; Busbey, 1995). The interlocking, radial pattern of the ridges, and grooves on the symphyseal plate also provide a mechanism to resist torsion at the mandibular symphysis.

Meckel's cartilage is a hyaline cartilage rod that forms the scaffold for the bony mandible during the development of the 1st branchial arch. As a result, Meckel's cartilage is understood to play an important role in mandibular morphogenesis, ossification, pathology, and evolution (Bellairs and Kamal, 1981; Rodriguez-Vasquez et al., 1997; Richman et al., 2006; Eames and Schneider, 2009; Ishizeki et al., 2010; Wu, 2011). Meckel's cartilage undergoes two fundamental evolutionary trajectories among vertebrates. In nonmammalian clades, such as alligators, Meckel's cartilage gives rise to the endochondrally ossified articular and quadrate, but remains through ontogeny

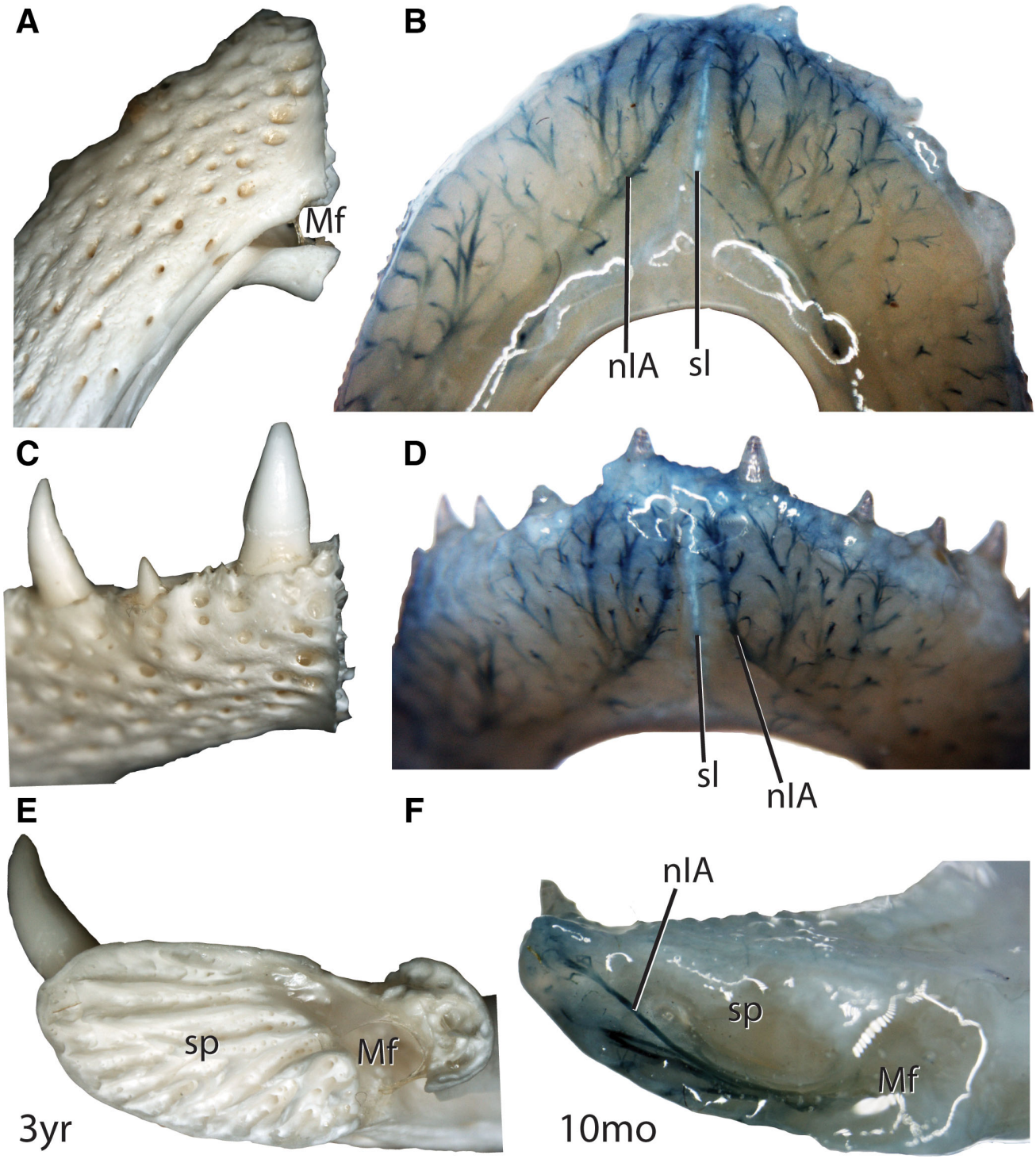

Fig. 6. Pictures of the left half of the opaque bony mandibular symphysis of 3 year MUVC AL1 in ventral (**A**), axial (**C**), and medial (**E**) views, and 10 month MUVC AL809 after clearing and Sudan Black B staining of myelinated nerves within the mandibles in ventral (**B**), axial (**D**), and medial (**F**) views.

as a persistent cartilaginous rod associated with the intramembranously ossified mandibular bones. In mammals, portions of Meckel's cartilage similarly cavitate into the ossicles of the inner ear, the tympanic ring of the ear, and the sphenomandibular ligament, and the remaining intramandibular portion recedes and disappears early in ontogeny once the dentary ossifies (see Wu, 2011 for a review), even among species with fused or unfused mandibular symphyses (Scapino 1981; Ravosa and Hogue, 2004; Scott et al., 2012). Mammalian Meckel's cartilage

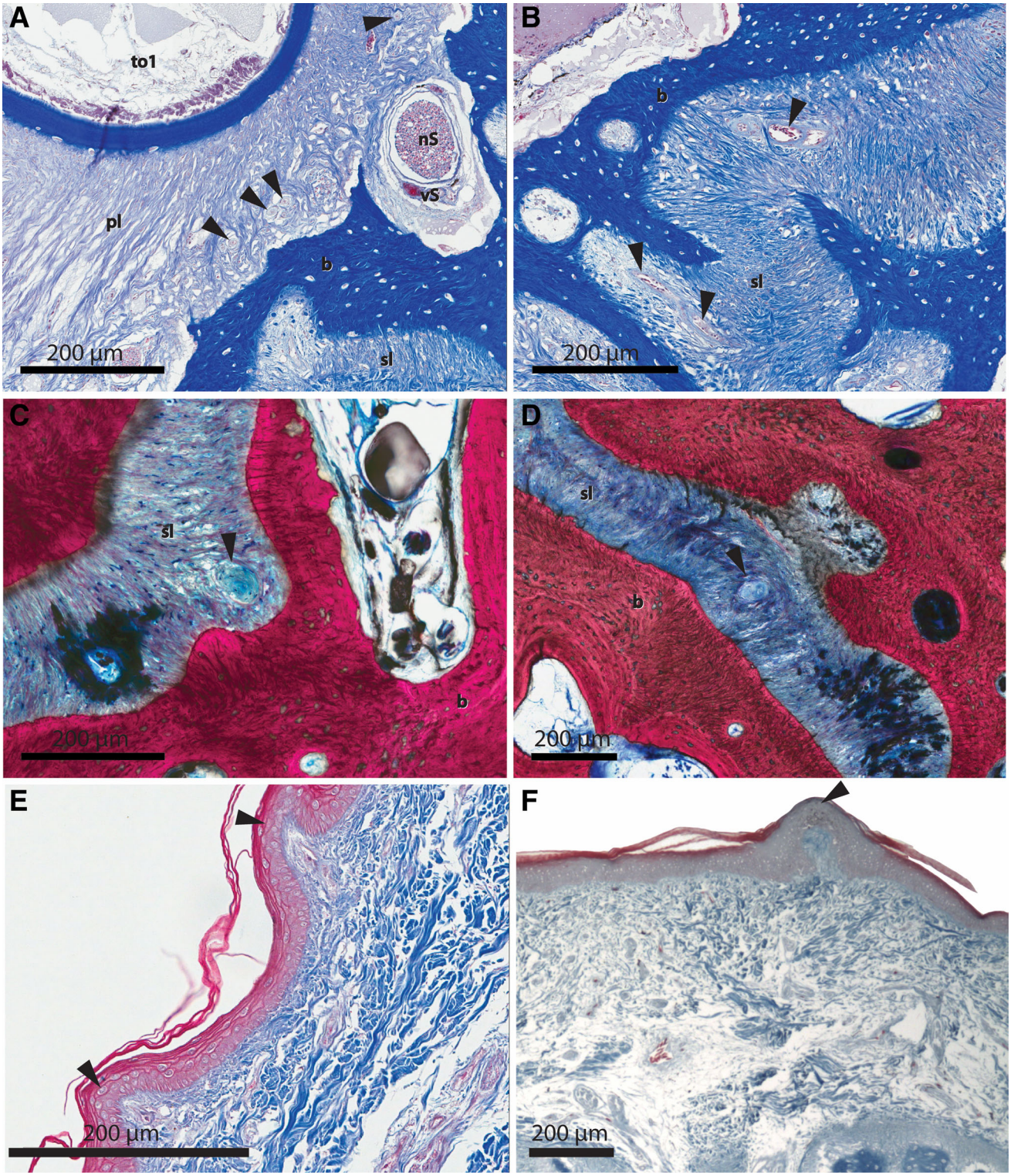

Fig. 7. Mechanoreceptors (arrows) within an alveolus of 3 month MUVC AL32 (**A**), vasculature (arrows) within the sutural ligament of 3 month MUVC AL32 (**B**), potential mechanoreceptors (arrows) within the sutural ligament of 3 year MUVC AL1 (**C**, **D**), and innervated integumentary sensory organs (arrows) from 3 month MUVC AL32 (**E**) and unknown age MUVC AL106 (**F**). Scale bars = 200 µm. Anatomical abbreviations in Table 2.

never persists in the adult form, but different developmental trajectories include growth of Meckel's cartilage without fusion, rostral fusion of the cartilaginous rods, and rostral fusion with growth of a rostral cartilaginous process (Lee et al., 2018). Similarly, although most sauropsid vertebrates (turtles, lizards, archosaurs) maintain the

primitive condition—a persistent cartilaginous rod within the bony mandible—only select taxa (e.g., geckos and crocodylians) fuse Meckel's cartilages at the symphysis (Holliday et al., 2010, Holliday and Nesbitt, 2013). Fusion of Meckel's cartilage creates a mixed syndesmodial and synchondroidal joint and a novel model system to study joint formation, cartilage fusion, and potentially cartilage repair. Cartilage fusion is a novel and poorly studied phenomenon, yet holds significant potential for understanding the new tissue-level mechanisms responsible for this fusion, the mechanical environment the cartilage experiences, and the significance it holds for the development, function, evolution, and even repair of the vertebrate skull.

During ontogeny, there is an overall trend of increasing complexity and organization within the alligator symphysis. Meckel's cartilage fuses, bone ossifies, collagen fibers in the sutural ligament align, and the suture takes on a characteristic interdigitating form. Whereas the symphysis of the embryonic *A. mississippiensis* resembles the Class I and II symphyses of squamates (*sensu* Scapino (1981) and Holliday and Nesbitt (2013)), it transforms into complicated Class III symphysis by 3 months posthatching. This transition to a more complicated morphology likely parallels the dietary shifts and increases in bite force that occur during ontogeny in alligator (Erickson et al., 2003).

Comparing across Crocodylia, the Meckel's cartilage of a Stage 22–25 *Crocodylus niloticus madagascariensis* embryo (from Handschuh et al., 2010) and a *Crocodylus porosus* embryo with a skull length of 15 mm (Shiino, 1914) is not dorsoventrally compressed rostrally nor is there a distinct spatulate process as in *A. mississippiensis* (Fig. 8). Additionally, the cartilaginous rods do not appear to be fully fused until their rostralmost extent in the embryonic *Crocodylus* specimens, and retain a septum similar to that present in iguanians (Holliday et al., 2010). Also, the Meckelian fossa terminates without dorsoventral compression in a more ventral position (i.e., medial to the roots of the rostral most teeth) in adult *Crocodylus* specimens as compared to *A. mississippiensis* (Fig. 8). Symphyseal length is variable among crocodylians, and the longisymphyseal members (e.g., *Gavialis* and *Tomistoma*) experience higher strains relative to brevisymphyseal members (e.g., *Alligator* and *Caiman*) (Walmsley et al., 2013). Therefore, if Meckel's cartilage plays a role in symphyseal strengthening, we expect decreased fusion of Meckel's cartilage in the longisymphyseal crocodylians. In some lizard taxa, Meckel's cartilage fuses during embryonic development only to later separate in adults (Holliday et al., 2010). This is in contrast to the development of the mandibular symphysis in *A. mississippiensis*, in which Meckel's cartilage fuses very early in development and remains fused through adulthood.

The crocodylian mandibular symphysis likely participates in monitoring the mechanical state of the mandible, incorporating information from trigeminal-nerve-innervated receptors distributed throughout the joint (Fig. 7). Previous

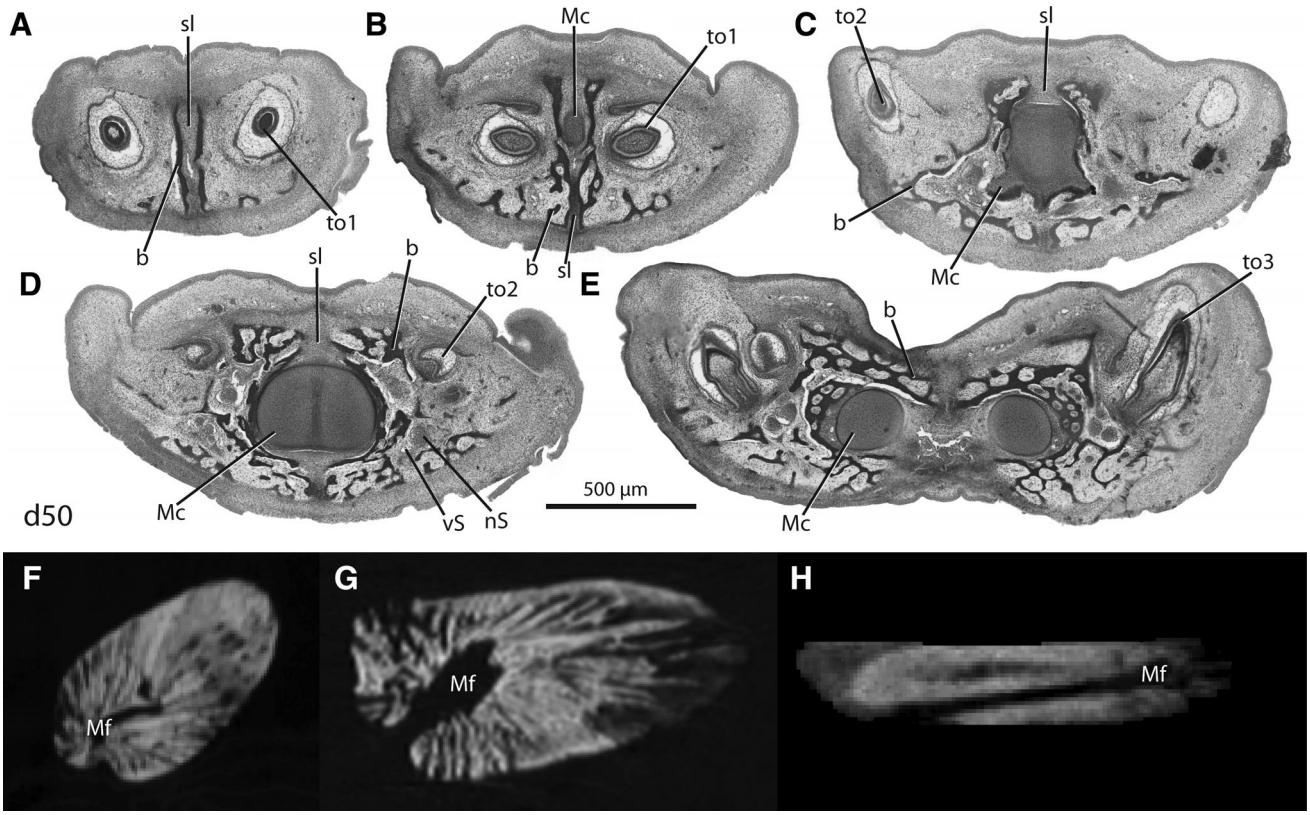

Fig. 8. Serial histological sections from the mandibular symphysis region of a 50 day *Crocodylus niloticus madagascariensis* embryo from Handschuh et al. (2010) in axial view from rostral (**A**) to caudal (**E**), and CT sections in midsagittal view of *Alligator mississippiensis* MUVC AL008 (**F**), *Crocodylus moreletii* TMM M-4980 (**G**), and *Crocodylus johnstoni* TMM M-6807 (**H**). Scale bar for A-E only = 0.5 mm. Anatomical abbreviations in Table 2.

research into the integumentary sensory organs of crocodylians has revealed these structures respond to mechanical, thermal, and chemical stimuli (Brazaitis, 1987; Soares, 2002; Leitch and Catania, 2012; Di-Poï and Milinkovitch, 2013). There is an increased density of integumentary sensory organs at the rostral margins of the mandible near the mandibular symphysis and adjacent to the teeth (Leitch and Catania, 2012; Fig. 3) reflecting the importance of this joint as a detector of external conditions. Our discovery of potential mechanoreceptors within the *Alligator* sutural ligament and confirmation of mechanoreceptors within the periodontal ligament along the symphysis support the hypothesis that the *Alligator* mandibular symphysis is a highly proprioceptive unit as well. Mechanoreceptors have been previously noted within the periodontal ligament of the crocodylian *Caiman sclerops* (Berkovitz and Sloan, 1978), and an investigation of forces perceived by receptors within the periodontal ligament suggests that these receptors are receptive to manipulation of the teeth as well as forces affecting the symphysis (Ness, 1954). Discovery of a sensory organ containing vasculature and mechanoreceptors within the whale mandibular symphysis (Pyenson et al., 2012) supports the possibility that the mechanoreceptors within the *Alligator* mandibular symphysis assist in configuring the jaws during feeding.

ACKNOWLEDGEMENTS

The authors thank Ruth Elsey and the Rockefeller State Refuge and Missouri Animal Care & Use Committee for aid in procuring and housing alligators. Thanks to Stephan Handschuh for sharing *Crocodylus* data and Duncan Leitch for sharing Sudan Black B staining protocol. Thanks to the American Association of Anatomists for a Short-term Visiting Scholarship (to CMH) and Helen Coates (Guelph), Jack Ratliff, and the University of Missouri Veterinary Medicine Diagnostic Lab for histology services and training. Thanks to Tara Selly, Jim Schiffbauer, MizzoμX, Ashley Szydrozski, Tim Hoffman, the MU Department of Radiology, and the MU Biomolecular Imaging Center for CT scanning. Thanks to Callum Ross, Laura Porro, Sterling Nesbitt, Rebecca Skiljan, and Kaleb Sellers for discussion.

LITERATURE CITED

Bailleul AM, Holliday CM. 2017. Joint histology in *Alligator mississippiensis* challenges the identification of synovial joints in fossil archosaurs and inferences of cranial kinesis. Proc R Soc B 281:20170038.

Bellairs A'A. 1984. Closing address, with comments on the organ of Jacobson and the evolution of Squamata, and on the intermandibular connection in Squamata. In: Fergusion MWJ, editor. *Zoological society of London symposium 52*. London: Academic Press. p 665–683.

Bellairs A'A, Kamal AM. 1981. The chondrocranium and the developmentof the skull in recent reptiles. In: Gans C, Parsons T, editors. *Biology of the Reptilia*, Vol. 11 (Morphology F). New York, NY: Academic Press. p 1–263.

Brazaitis P. 1987. Identification of crocodilian skins and products. In: Webb GJ, Manolis SC, Whitehead PJ, editors. *Wildlife Management: Crocodiles and Alligators. Chipping Norton*. Australia: Surrey Beatty & Sons. p 373–386.

Berkovitz BKB, Sloan P. 1978. Attachment tissues of the teeth in *Caiman sclerops* (Crocodilia). J Zool 187:179–194.

Brochu CA. 2001. Crocodylian snouts in space and time: phylogenetic approaches toward adaptive radiation. Amer Zool 41:564–585.

Busbey AB. 1989. Form and function of the feeding apparatus of *Alligator mississippiensis*. J Morph 202:99–127.

Busbey AB. 1995. The structural consequences of skull flattening in crocodilians. In: Thomason J, editor. *Functional morphology in vertebrate paleontology*. New York, NY: Cambridge University Press. p 173–192.

Clark JM, Xu X, Forster CA, Wang Y. 2004. A Middle Jurassic 'sphenosuchian' from China and the origin of the crocodylian skull. Nature 430:1021–1024.

Currey JD. 2002. *The structure of bone tissue. Bones: Structure and Mechanics*. Princeton, NJ: Princeton University Press. p 1–436.

Di-Poï N, Milinkovitch MC. 2013. Crocodylians evolved scattered multi-sensory micro-organs. EvoDevo 4(1):19–15.

Eames BF, Schneider RA. 2009. The genesis of cartilage size and shape during development and evolution. Development 135:3947–3958.

Erickson GM, Lappin AK, Vliet KA. 2003. The ontogeny of bite-force performance in American alligator (*Alligator mississippiensis*). J Zool Lond 260:317–327.

Erickson GM, Gignac PM, Steppan SJ, Lappin AK, Vliet KA, Brueggen JD, Inouye BD, Kledzik D, Webb GJ. 2012. Insights into the ecology and evolutionary success of crocodilians revealed through bite-force and tooth-pressure experimentation. PLoS One 7:e31781.

Ferguson MWJ. 1985. Reproductive biology and embryology of the crocodilians. In: Gans C, Billet F, Maderson PFA, editors. *Biology of the Reptilia, vol 14, development A*. New York, NY: John Wiley & Sons. p 329–491.

Filipski GT, Wilson MVH. 1986. Nerve staining using Sudan Black B and its potential use in comparative anatomy. In: Waddington J, Rudkin DM, editors. *Proceedings of the 1985 Workshop on Care and Maintenance of Natural History Collections*. Toronto: Royal Ontario Museum Life Sciences Miscellaneous Publication. p 33–36.

George ID, Holliday CM. 2013. Trigeminal nerve morphology in *Alligator mississippiensis* and its significance for crocodyliform facial sensation and evolution. Anat Rec 296:670–680.

Gignac PM, Kley NJ, Clarke JA, Colbert MW, Morhardt AC, Cerio D, Cost IN, Cox PG, Daza JD, Early CM, et al. 2016. Diffusible iodine-based contrast-enhanced computed tomography (diceCT): an emerging tool for rapid, high-resolution, 3-D imaging of metazoan soft tissues. J Anat 228:889–909.

Handschuh S, Schwaha T, Metscher BD. 2010. Showing their true colors : a practical approach to volume rendering from serial sections. BMC Dev Biol 10:41.

Herring SW, Rafferty KL, Zi JL, Sun Z. 2008. A non primate model for the fused symphysis: in vivo studies in the pig. In: Vinyard C, Ravosa MJ, Wall C, editors. *Primate craniofacial function and biology*. New York, NY: Springer. p 19–38.

Hogg DA. 1983. Fusions within the mandible of the domestic fowl (*Gallus Gallus domesticus*). J Anat 136:535–541.

Hogue AS, Ravosa MJ. 2001. Transverse masticatory movements, occlusal orientation, and symphyseal fusion in slenodont artiodactyls. J Morphol 159:253–296.

Holliday CM, Gardner NM, Paesani SM, Douthitt M, Ratliff JL. 2010. Microanatomy of the mandibular symphysis in lizards: patterns in fiber orientation and Meckel's cartilage and their significance in cranial evolution. Anat Rec 293:1350–1359.

Holliday CM, Nesbitt SJ. 2013. Morphology and diversity of the mandibular symphysis of archosauriforms. Geol Soc Lond Spec Publ 379:555–571.

Ishizeki K, Tadayoshi K, Fujiwara N, Otsu K, Hidemitsu H. 2010. Biological significance of site-specific transformation of chondrocytes in mouse Meckel's cartilage. J Oral Biosci 52:136–142.

Jacoby MJ, Gant CA, Sellers KC, Holliday CM. 2015. Ontogeny and complexity of the mandibular symphysis of crocodylians. Society for Integrative and Comparative Biology 2015 Annual Meeting Abstracts. p 156.

Junqueira LC, Bignolas G, Brentani RR. 1979. Picrosirius staining plus polarization microscopy, a specific method for collagen detection in tissue sections. Histochem J 11:447–455.

Kellogg R. 1929. The habits and economic importance of alligators. Tech Bull USDA 147:1–36.

Kley NJ. 2006. Morphology of the lower jaw and suspensorium in the Texas blindsnake, *Leptotyphlops dulcis* (Scolecodphidia: Leptotyphlopidae). 267:494–515.

Langston WJR. 1973. The crocodilian skull in historical perspective. In: Gans C, Parsons TS, editors. *Biology of the Reptilia*, Vol. 4 (Morphology D). New York, NY: Academic Press. p 263–284.

Lee E, Popowics T, Herring SW. 2018. Histological development of the fused mandibular symphysis in the pig. Anat Rec, Early view. https://doi.org/10.1002/ar.23993.

Leitch DB, Catania KC. 2012. Structure, innervation and response properties of integumentary sensory organs in crocodilians. J Exp Biol 215:4217–4230.

McLean KE, Vickaryous MK. 2011. A novel amniote model of epimorphic regeneration: the leopard gecko, *Eublepharis macularius*. BMC Dev Biol 11:50.

Ness AR. 1954. The mechanoreceptors of the rabbit mandibular incisor. J Physiol 126:475–493.

Nobre PH, de Souza Carvalho I, de Vasconcellos FM, Souto PR. 2008. Feeding behavior of the Gondwanic Crocodylomorpha *Mariliasuchus amarali* from the Upper Cretaceous Bauru Basin, Brazil. Gondw Res 13:139–145.

O'Connor PM, Sertich JJ, Stevens NJ, Roberts EM, Gottfried MD, Hieronymus TL, Jinnah ZA, Ridgely R, Ngasala SE, Temba J. 2010. The evolution of mammal-like crocodyliforms in the Cretaceous Period of Gondwana. Nature 466:748–751.

Ősi A, Weishampel DB. 2009. Jaw mechanism and dental function in the Late Cretaceous basal eusuchian *Iharkutosuchus*. J Morph 270:903–920.

Parker WK. 1883. On the structure and development of the skull in the Crocodilia. Trans Zool Soc Lond 11:263–310.

Payne SL, Holliday CM, Vickaryous MK. 2011. An osteological and histological investigation of cranial joints in geckos. Anat Rec 294: 399–405.

Porro LB, Holliday CM, Anapol F, Ontiveros LC, Ontiveros LT, Ross CF. 2011. Free body analysis, beam mechanics, and finite element modeling of the mandible of *Alligator mississippiensis*. 937:910–937.

Porro LB, Metzger KA, Iriarte-Diaz J, Ross CF. 2013. In vivo bone strain and finite element modeling of the mandible of *Alligator mississippiensis*. J Anat 223:195–227.

Porter WR, Sedlmayr JC, Witmer LM. 2016. Vascular patterns in the heads of crocodilians: blood vessels and sites of thermal exchange. J Anat 229:800–824.

Pyenson ND, Goldbogen JA, Vogl AW, Szathmary G, Drake RL, Shadwick RE. 2012. Discovery of a sensory organ that coordinates lunge feeding in rorqual whales. Nature 485:489–501.

Rafferty KL, Herring SW. 1999. Craniofacial sutures: morphology, growth, and in vivo masticatory strains. J Morphol 242:167–179.

Ravosa MJ, Hogue AS. 2004. Function and fusion of the mandibular symphysis in mammals: a comparative and experimental perspective. In: Ross CV, Kay RF, editors. *Anthropoid origins*. Boston: Springer. p 413–462.

Richman JM, Cuchtova M, Boughner JC. 2006. Comparative ontogeny and phylogeny of the upper jaw skeleton in Amniotes. Devel Dyn 235:1230–1243.

Rodriguez-Vasquez FJ, Merida-Velasco JR, Merida-Velasco JA, Sanchez-Montesinos I, Espin- Ferra J, Jimeneaz-Collado J. 1997. Development of Meckel's cartilage in the symphyseal region in man. Anat Rec 249:249–254.

Sellers KC, Middleton KM, Davis JL, Holliday CM. 2017. Ontogeny of bite force in a validated biomechanical model of the American alligator. J Experim Biol 220:2036–2046.

Scapino RP. 1981. Morphological investigation into functions of the jaw symphysis in carnivorans. J Morphol 167:339–375.

Scott JE, Hogue AS, Ravosa MJ. 2012. The adaptive significance of mandibular symphyseal fusion in mammals. J Evol Biol 25: 661–673.

Shiino K. 1914. Das chondrocranium von crocodilus mit berücksichtigung der gehirnnerven und der kopfgefässe. Anat Hefte 50: 253–382.

Soares D. 2002. Neurology: an ancient sensory organ in crocodilians. Nature 417:241–242.

Stubbs TL, Pierce SE, Rayfield EJ, Anderson PSL. 2013. Morphological and biomechanical disparity of crocodile-line archosaurs following the end-Triassic extinction. Proc R Soc B 280:20131940.

Svensson ME, Haas A. 2005. Evolutionary innovation in the vertebrate jaw: a derived morphology in anuran tadpoles and its possible developmental origin. Bioessays 27:526–532.

Walmsley CW, Smits PD, Quayle MR, Mccurry MR, Richards HS, Oldfield CC, Wroe S, Clausen PD, Mchenry CR. 2013. Why the long face? The mechanics of mandibular symphysis proportions in crocodiles. PLoS One 16:e53873.

Williams SH, Wall CE, Vinyard CJ, Hylander WL. 2008. Symphyseal fusion in selenodont artiodactyls: new insights from in vivo and comparative data. In: Vinyard C, Ravosa MJ, Wall C, editors. *Primate craniofacial function and biology*. New York, NY: Springer. p 39–61.

Witten PE, Hall BK. 2003. Seasonal changes in the lower jaw skeleton in male Atlantic salmon (*Salmo salar* L.): remodelling and regression of the kype after spawning. J Anat 203:435–450.

Wu Z. 2011. Developmental patterns in Mesozoic evolution of mammal ears. Ann Rev Eco Evol Syst 42:355–380.